Guaranteed Lower and Upper Bounds on the Finite-Frequency H 2 Norm of Uncertain Linear Systems

Tommaso Casati, Clément Roos, Jean-Marc Biannic, Hélène Evain

Guaranteed Lower and Upper Bounds on the Finite-Frequency H_2 Norm of Uncertain Linear Systems

Tommaso Casati[1*], Clément Roos[1], Jean-Marc Biannic[1], Hélène Evain[2]

***Abstract*— The H_2 norm plays a key role in control applications when the input of the system is a random noise. It is therefore important to evaluate how this metric is affected by uncertainties in the model. Different approaches have been proposed in the literature to compute an upper bound on the worst-case H_2 norm of an uncertain system. No method, however, is available to check if the H_2 norm remains larger than a given threshold on an entire set of uncertainties. In this context, the present paper introduces a sufficient condition to compute a guaranteed lower bound on the H_2 norm of an uncertain system based on Linear Matrix Inequalities (LMIs). G-scaling matrices are also introduced to improve the accuracy of the computed bounds in presence of real parametric uncertainties. The theoretical results are implemented and applied to test cases of increasing complexity.**

Keywords: H_2 norm, Uncertain systems, Robust performance, Space applications

I. INTRODUCTION

The H_2 norm represents a crucial design metric for many applications, involving structural dynamics, micro-vibrations, acoustics and coloured noise rejection issues [1]. This metric is particularly useful when the input of the system is a stochastic noise. For example, Alazard used H_2 synthesis to perform lateral flight control design for a flexible aircraft [2]. Cracciolo et al. developed a mixed H_2/H_∞ optimization procedure to control the vibrations of flexible link mechanisms [3]. Zattoni studied the condition monitoring of electric switch machines for railway points by treating the electrical noise with an H_2-norm type criterion [4]. Martin et al. analyzed the H_2 performance of a spacecraft lander in an uncertain environment around a small solar system body [5]. Navarro-Tapia et al. proposed an H_2-based verification framework to evaluate the pointing performance of high-accuracy space missions in presence of disturbances and uncertainties [6].

Generally, the computation of the worst-case H_2 norm of an uncertain system is NP hard, so bounds are determined instead. Different approaches have been proposed in the literature to compute an upper bound. Paganini proposed both frequency-domain and state-space conditions to analyze H_2 performance [7], [8]. Both methods require to solve a SemiDefinite Programming (SDP) optimization problem, subject to Linear Matrix Inequalities (LMIs). The state-space based approach calculates an upper bound using a single LMI, but the dimension of the problem rapidly grows with the number of states. For the frequency-based approach, the number of decision variables depends only on the number of uncertainties and their occurences in the model, but the number of LMIs is infinite. In practice, the problem is solved on a finite frequency grid, and a Hamiltonian-based technique inspired by [9], [10] is proposed in [1] to validate the solution on the entire frequency range. Among other approaches, Scherer et al. tackled the robust H_2 estimator design problem by using Integral Qudratic Contraints (IQCs) [11], [12]. The resulting frequency-domain inequalities are cast into state-space LMIs through the Kalman-Yakubovich-Popov (KYP) lemma. Veenman et al. developed an IQC-based toolbox called IQClab which evaluates the H_2 performance of uncertain systems for robustness analysis and control design purposes [13]. Preda calculated an upper bound on the robust H_2 norm by reformulating the problem as a standard worst-case L_2 calculation [14]. A similar concept was also proposed by Martin et al., who traced the robust H_2-norm computation back to the structured singular value [5].

In contrast, the present paper proposes a method to compute a lower bound on the finite-frequency H_2 norm of an uncertain Multiple-Input Multiple-Output (MIMO) system, a problem for which there is currently no solution to the authors' knowledge. This guarantees that the system performance is not satisfied in certain regions of the uncertainty domain, which, beyond invalidating the controller, also provides essential information for improving the design. Following the approach of [7], new frequency-dependent LMIs are first derived, which guarantee that an H_2 performance requirement is violated. The Hamiltonian-based technique of [1] is then adapted to deal with this violation condition. G-scaling matrices are also introduced, which significantly increases the accuracy of the bounds in the presence of real parametric uncertainties [15].

The paper is organized as follows. Some preliminaries to the H_2 performance problem are first discussed in Section II. A sufficient lower bound condition is then demonstrated in Section III and the Hamiltonian-based approach is adapted accordingly in Section IV. Eventually, the theoretical results are implemented in Section V and applied to test cases of increasing complexity in Section VI.

Notation

The notation used in the paper is standard. Bold font is adopted for vectors and matrices, whereas roman characters indicate scalars. $\mathbb{R}$ represents the real space. Supremum and infinimum of a set or a function are denoted $\sup$ and $\inf$ respectively. Given a matrix $\boldsymbol{A}$, $\boldsymbol{A}'$ is its transpose and $\boldsymbol{A}^*$ its conjugate transpose. $\boldsymbol{I}$ stands for the identity matrix.

*Corresponding author: tommaso.casati@onera.fr
[1]DTIS, ONERA, Université de Toulouse, 31000 Toulouse France
[2]CNES - The French Space Agency, 31400 Toulouse France

The inequality relations between hermitian matrices are expressed by $\preccurlyeq$, $\prec$, $\succcurlyeq$ and $\succ$. Given n matrices $\{\boldsymbol{A}_i\}_{i=1,\ldots,n}$, $\mathrm{diag}\left(\boldsymbol{A}_1,\ldots,\boldsymbol{A}_n\right)$ denotes the standard block-diagonal augmentation. The transfer matrix of a system in terms of its state-space representation is expressed as

$$\left[\begin{array}{c|c} \boldsymbol{A} & \boldsymbol{B} \\ \hline \boldsymbol{C} & \boldsymbol{D} \end{array}\right] = \boldsymbol{C}\left(s\boldsymbol{I}-\boldsymbol{A}\right)^{-1}\boldsymbol{B}+\boldsymbol{D} \tag{1}$$

$||\cdot||$ and $||\cdot||_2$ indicate respectively the Euclidean norm and the H_2 norm.

II. PRELIMINARIES

A. Definitions

Consider the uncertain MIMO linear system of Fig. 1, where the transfer matrix between $\boldsymbol{u}$ and $\boldsymbol{y}$ corresponds to the upper Linear Fractional Transformation (LFT) $\boldsymbol{\mathcal{F}}_u\left(\boldsymbol{M}\left(s\right),\boldsymbol{\Delta}\left(s\right)\right)$.

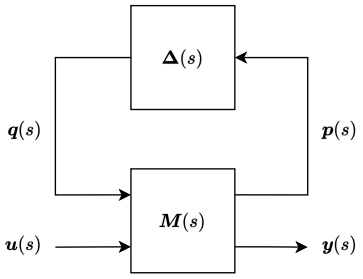

Fig. 1. LFT representation of an uncertain system.

$\boldsymbol{M}\left(s\right)$ is a continuous-time, stable and proper real-rational transfer matrix representing the nominal closed-loop system. $\boldsymbol{\Delta}\left(s\right)=\mathrm{diag}\left(\boldsymbol{\Delta}_1\left(s\right),\ldots,\boldsymbol{\Delta}_N\left(s\right)\right)$ is a structured block-diagonal Linear Time-Invariant (LTI) operator which gathers all model uncertainties. Each $\boldsymbol{\Delta}_i\left(s\right)$ can be:

- a time-invariant diagonal matrix $\boldsymbol{\Delta}_i\left(s\right)=\delta_i\boldsymbol{I}$, where δ_i is a real or a complex parametric uncertainty,
- or a stable and proper real-rational unstructured transfer matrix usually representing neglected dynamics [16].

The set of all admissible uncertainties $\mathbb{\Delta}$ is such that $\forall\omega\in\mathbb{R}$, $\boldsymbol{\Delta}\left(j\omega\right)\in\mathbb{\Delta}$ or (with a slight abuse of notation) $\boldsymbol{\Delta}\left(s\right)\in\mathbb{\Delta}$ [16]. Let then $\boldsymbol{B}_{\mathbb{\Delta}}=\{\boldsymbol{\Delta}\in\mathbb{\Delta}:\bar{\sigma}\left(\boldsymbol{\Delta}\right)\leq 1\}$, where $\bar{\sigma}\left(\boldsymbol{\Delta}\right)$ denotes the largest singular value of $\boldsymbol{\Delta}$ [16]. For any admissible $\boldsymbol{\Delta}\left(s\right)\in\mathbb{\Delta}$, the H_2 norm of the transfer matrix $\boldsymbol{\mathcal{F}}_u\left(\boldsymbol{M}\left(s\right),\boldsymbol{\Delta}\left(s\right)\right)$, assumed strictly proper, is defined as in [17]:

$$\begin{aligned}&||\boldsymbol{\mathcal{F}}_u\left(\boldsymbol{M}\left(s\right),\boldsymbol{\Delta}\left(s\right)\right)||_2\\ &:=\left(\int_{-\infty}^{\infty}\mathrm{tr}\left(\boldsymbol{\mathcal{F}}_u\left(j\omega\right)\boldsymbol{\mathcal{F}}_u\left(j\omega\right)^*\right)\frac{d\omega}{2\pi}\right)^{1/2}\end{aligned} \tag{2}$$

where $\boldsymbol{\mathcal{F}}_u\left(j\omega\right)$ is written instead of $\boldsymbol{\mathcal{F}}_u\left(\boldsymbol{M}\left(j\omega\right),\boldsymbol{\Delta}\left(j\omega\right)\right)$ to simplify. Note that Eq. (2) corresponds to the root mean square norm of the output $\boldsymbol{y}$ when the input $\boldsymbol{u}$ is a unitary white noise. This metric, therefore, gives an idea of how a random signal would be amplified by the system. Similarly, the finite-frequency H_2 norm of the transfer matrix $\boldsymbol{\mathcal{F}}_u\left(\boldsymbol{M}\left(s\right),\boldsymbol{\Delta}\left(s\right)\right)$ is defined as

$$\begin{aligned}&||\boldsymbol{\mathcal{F}}_u\left(\boldsymbol{M}\left(s\right),\boldsymbol{\Delta}\left(s\right)\right)||_{2,\bar{\omega}}\\ &:=\left(\int_{-\bar{\omega}}^{\bar{\omega}}\mathrm{tr}\left(\boldsymbol{\mathcal{F}}_u\left(j\omega\right)\boldsymbol{\mathcal{F}}_u\left(j\omega\right)^*\right)\frac{d\omega}{2\pi}\right)^{1/2}\end{aligned} \tag{3}$$

where $\bar{\omega}\in[0,+\infty)$ [1]. Note that in this case, $\boldsymbol{\mathcal{F}}_u\left(\boldsymbol{M}\left(s\right),\boldsymbol{\Delta}\left(s\right)\right)$ does not need to be strictly proper.

B. Problem Formulation

The present paper investigates how the H_2 performance of a system is affected by uncertainties in the model. Different methods have been proposed in the literature to compute an upper bound γ_u on $||\boldsymbol{\mathcal{F}}_u\left(\boldsymbol{M}\left(s\right),\boldsymbol{\Delta}\left(s\right)\right)||_{2,\bar{\omega}}$ when $\boldsymbol{\Delta}$ is a LTI operator:

$$\sup_{\boldsymbol{\Delta}\in\boldsymbol{B}_{\mathbb{\Delta}}}||\boldsymbol{\mathcal{F}}_u\left(\boldsymbol{M}\left(s\right),\boldsymbol{\Delta}\left(s\right)\right)||_{2,\bar{\omega}}<\gamma_u \tag{4}$$

No technique, however, is available to determine if the H_2 performance is violated for all uncertainties in a given set. In this context, the paper demonstrates a sufficient condition to identify a guaranteed lower bound γ_l on $||\boldsymbol{\mathcal{F}}_u\left(\boldsymbol{M}\left(s\right),\boldsymbol{\Delta}\left(s\right)\right)||_{2,\bar{\omega}}$ such that

$$\inf_{\boldsymbol{\Delta}\in\boldsymbol{B}_{\mathbb{\Delta}}}||\boldsymbol{\mathcal{F}}_u\left(\boldsymbol{M}\left(s\right),\boldsymbol{\Delta}\left(s\right)\right)||_{2,\bar{\omega}}>\gamma_l \tag{5}$$

III. UPPER AND LOWER H_2-NORM BOUNDS

This section proposes a method to calculate guaranteed upper and lower bounds γ_u and γ_l on the finite-frequency H_2 norm of an uncertain system.

A. Upper bound

Let $\mathbb{X}=\{\boldsymbol{X}=\boldsymbol{X}^*\succ\boldsymbol{0}:\forall\boldsymbol{\Delta}\in\mathbb{\Delta},\boldsymbol{X}\boldsymbol{\Delta}=\boldsymbol{\Delta}\boldsymbol{X}\}$ be the set of hermitian, positive definite matrices $\boldsymbol{X}$ which commute with $\boldsymbol{\Delta}$. Let also $\mathbb{G}=\{\boldsymbol{G}=\boldsymbol{G}^*:\forall\boldsymbol{\Delta}\in\mathbb{\Delta},\boldsymbol{G}\boldsymbol{\Delta}=\boldsymbol{\Delta}^*\boldsymbol{G}\}$ be the set of hermitian G-scaling matrices. The following theorem is an adaptation of [7] where real parametric uncertainties are classically handled through the use of G scalings as is proposed in the well-known characterization of the mixed-μ upper bound [15]. The demonstration follows that of [7] and it is similar to the proof of Theorem 2. It is then omitted for brevity.

Theorem 1: Suppose there exist $\boldsymbol{X}\left(\omega\right)\in\mathbb{X}$, $\boldsymbol{G}\left(\omega\right)\in\mathbb{G}$, $\boldsymbol{Y}\left(\omega\right)=\boldsymbol{Y}\left(\omega\right)^*$ and $\gamma_u>0$ such that

$$\begin{aligned}&\boldsymbol{M}\left(j\omega\right)^*\begin{bmatrix}\boldsymbol{X}\left(\omega\right)&\boldsymbol{0}\\ \boldsymbol{0}&\boldsymbol{I}\end{bmatrix}\boldsymbol{M}\left(j\omega\right)\\ &+j\left(\begin{bmatrix}\boldsymbol{G}\left(\omega\right)&\boldsymbol{0}\\ \boldsymbol{0}&\boldsymbol{0}\end{bmatrix}\boldsymbol{M}\left(j\omega\right)-\boldsymbol{M}\left(j\omega\right)^*\begin{bmatrix}\boldsymbol{G}\left(\omega\right)&\boldsymbol{0}\\ \boldsymbol{0}&\boldsymbol{0}\end{bmatrix}\right)\\ &-\begin{bmatrix}\boldsymbol{X}\left(\omega\right)&\boldsymbol{0}\\ \boldsymbol{0}&\boldsymbol{Y}\left(\omega\right)\end{bmatrix}\prec\boldsymbol{0}\quad\forall\omega\in[-\bar{\omega},\bar{\omega}]\end{aligned} \tag{6}$$

and

$$\int_{-\bar{\omega}}^{\bar{\omega}}\mathrm{tr}\left(\boldsymbol{Y}\left(\omega\right)\right)\frac{d\omega}{2\pi}<\gamma_u^2 \tag{7}$$

Then

$$\sup_{\boldsymbol{\Delta}\in\boldsymbol{B}_{\mathbb{\Delta}}}||\boldsymbol{\mathcal{F}}_u\left(\boldsymbol{M}\left(s\right),\boldsymbol{\Delta}\left(s\right)\right)||_{2,\bar{\omega}}<\gamma_u \tag{8}$$

B. Lower Bound

This subsection proposes a similar approach to compute a lower bound on the frequency-limited H_2 norm of an uncertain system, which is the first contribution of this paper.

Theorem 2: Suppose there exist $\boldsymbol{X}(\omega) \in \mathbb{X}$, $\boldsymbol{G}(\omega) \in \mathbb{G}$, $\boldsymbol{Y}(\omega) = \boldsymbol{Y}(\omega)^*$ and $\gamma_l > 0$ such that

$$\begin{aligned} &\boldsymbol{M}(j\omega)^* \begin{bmatrix} -\boldsymbol{X}(\omega) & \boldsymbol{0} \\ \boldsymbol{0} & \boldsymbol{I} \end{bmatrix} \boldsymbol{M}(j\omega) \\ &+j\left(\begin{bmatrix} \boldsymbol{G}(\omega) & \boldsymbol{0} \\ \boldsymbol{0} & \boldsymbol{0} \end{bmatrix} \boldsymbol{M}(j\omega) - \boldsymbol{M}(j\omega)^* \begin{bmatrix} \boldsymbol{G}(\omega) & \boldsymbol{0} \\ \boldsymbol{0} & \boldsymbol{0} \end{bmatrix} \right) \\ &- \begin{bmatrix} -\boldsymbol{X}(\omega) & \boldsymbol{0} \\ \boldsymbol{0} & \boldsymbol{Y}(\omega) \end{bmatrix} \succ \boldsymbol{0} \quad \forall \omega \in [-\bar{\omega}, \bar{\omega}] \end{aligned} \tag{9}$$

and

$$\int_{-\bar{\omega}}^{\bar{\omega}} \operatorname{tr}(\boldsymbol{Y}(\omega)) \frac{d\omega}{2\pi} > \gamma_l^2 \tag{10}$$

Then

$$\inf_{\boldsymbol{\Delta} \in \boldsymbol{B}_{\triangle}} ||\boldsymbol{\mathcal{F}}_u(\boldsymbol{M}(s), \boldsymbol{\Delta}(s))||_{2,\bar{\omega}} > \gamma_l \tag{11}$$

Proof: Let $\boldsymbol{M} = \boldsymbol{M}(j\omega)$, $\boldsymbol{X} = \boldsymbol{X}(\omega)$, $\boldsymbol{G} = \boldsymbol{G}(\omega)$ and $\boldsymbol{Y} = \boldsymbol{Y}(\omega)$. Let also $\boldsymbol{p} = \boldsymbol{p}(j\omega)$, $\boldsymbol{q} = \boldsymbol{q}(j\omega)$, $\boldsymbol{u} = \boldsymbol{u}(j\omega)$ and $\boldsymbol{y} = \boldsymbol{y}(j\omega)$ be the vectors reported in Fig. 1. Define $\tilde{\boldsymbol{D}}_+ = \begin{bmatrix} \boldsymbol{X}^{1/2} & \boldsymbol{0} \\ \boldsymbol{0} & \boldsymbol{I} \end{bmatrix}$, $\tilde{\boldsymbol{D}}_- = \begin{bmatrix} -\boldsymbol{X}^{1/2} & \boldsymbol{0} \\ \boldsymbol{0} & \boldsymbol{I} \end{bmatrix}$, $\tilde{\boldsymbol{G}} = \begin{bmatrix} \boldsymbol{G} & \boldsymbol{0} \\ \boldsymbol{0} & \boldsymbol{0} \end{bmatrix}$ and $\tilde{\boldsymbol{Y}} = \begin{bmatrix} -\boldsymbol{I} & \boldsymbol{0} \\ \boldsymbol{0} & \boldsymbol{Y} \end{bmatrix}$. Eq. (9) can be accordingly expressed as

$$\begin{aligned} &\tilde{\boldsymbol{D}}_+^{-1} \boldsymbol{M}^* \tilde{\boldsymbol{D}}_- \tilde{\boldsymbol{D}}_+ \boldsymbol{M} \tilde{\boldsymbol{D}}_+^{-1} \\ &+j\left(\tilde{\boldsymbol{D}}_+^{-1} \tilde{\boldsymbol{G}} \boldsymbol{M} \tilde{\boldsymbol{D}}_+^{-1} - \tilde{\boldsymbol{D}}_+^{-1} \boldsymbol{M}^* \tilde{\boldsymbol{G}} \tilde{\boldsymbol{D}}_+^{-1} \right) - \tilde{\boldsymbol{Y}} \succ \boldsymbol{0} \end{aligned} \tag{12}$$

Define $\bar{\boldsymbol{q}} = \boldsymbol{X}^{1/2}\boldsymbol{q}$ and $\bar{\boldsymbol{p}} = \boldsymbol{X}^{1/2}\boldsymbol{p}$. By pre and post multiplying both sides of Eq. (12) by $\begin{bmatrix} \bar{\boldsymbol{q}} \\ \boldsymbol{u} \end{bmatrix}^*$ and $\begin{bmatrix} \bar{\boldsymbol{q}} \\ \boldsymbol{u} \end{bmatrix}$ respectively, and considering that $\tilde{\boldsymbol{D}}_+^{-1} \begin{bmatrix} \bar{\boldsymbol{q}} \\ \boldsymbol{u} \end{bmatrix} = \begin{bmatrix} \boldsymbol{q} \\ \boldsymbol{u} \end{bmatrix}$, $\boldsymbol{M} \begin{bmatrix} \boldsymbol{q} \\ \boldsymbol{u} \end{bmatrix} = \begin{bmatrix} \boldsymbol{p} \\ \boldsymbol{y} \end{bmatrix}$ and $\tilde{\boldsymbol{D}}_+ \begin{bmatrix} \boldsymbol{p} \\ \boldsymbol{y} \end{bmatrix} = \begin{bmatrix} \bar{\boldsymbol{p}} \\ \boldsymbol{y} \end{bmatrix}$, Eq. (12) yields

$$||\boldsymbol{y}||^2 - ||\bar{\boldsymbol{p}}||^2 + \boldsymbol{q}^* \boldsymbol{G} \boldsymbol{p} - \boldsymbol{p}^* \boldsymbol{G} \boldsymbol{q} > -||\bar{\boldsymbol{q}}||^2 + \boldsymbol{u}^* \boldsymbol{Y} \boldsymbol{u} \tag{13}$$

As from Fig. 1 $\boldsymbol{q} = \boldsymbol{\Delta}\boldsymbol{p}$, $\boldsymbol{q}^*\boldsymbol{G}\boldsymbol{p} = \boldsymbol{p}^*\boldsymbol{\Delta}^*\boldsymbol{G}\boldsymbol{p}$ and $\boldsymbol{p}^*\boldsymbol{G}\boldsymbol{q} = \boldsymbol{p}^*\boldsymbol{G}\boldsymbol{\Delta}\boldsymbol{p}$. Knowing also that $\boldsymbol{G}\boldsymbol{\Delta} = \boldsymbol{\Delta}^*\boldsymbol{G}$, Eq. (13) can be simplified as follows:

$$||\boldsymbol{y}||^2 - ||\bar{\boldsymbol{p}}||^2 > -||\bar{\boldsymbol{q}}||^2 + \boldsymbol{u}^* \boldsymbol{Y} \boldsymbol{u} \tag{14}$$

Considering also that $\bar{\boldsymbol{q}} = \boldsymbol{X}^{1/2}\boldsymbol{q} = \boldsymbol{X}^{1/2}\boldsymbol{\Delta}\boldsymbol{X}^{-1/2}\bar{\boldsymbol{p}} = \boldsymbol{\Delta}\bar{\boldsymbol{p}}$ and $\boldsymbol{\Delta} \in \boldsymbol{B}_{\triangle}$ is contractive, Eq. (14) yields

$$||\boldsymbol{y}||^2 > \boldsymbol{u}^* \boldsymbol{Y} \boldsymbol{u} \tag{15}$$

Knowing from the definition of the LFT represented in Fig. 1 that $||\boldsymbol{y}(j\omega)||^2 = \boldsymbol{u}(j\omega)^* \boldsymbol{\mathcal{F}}_u(j\omega)^* \boldsymbol{\mathcal{F}}_u(j\omega) \boldsymbol{u}(j\omega)$, Eq. (15) becomes

$$\boldsymbol{\mathcal{F}}_u(j\omega)^* \boldsymbol{\mathcal{F}}_u(j\omega) > \boldsymbol{Y}(\omega) \tag{16}$$

Computing the trace and integrating gives

$$||\boldsymbol{\mathcal{F}}_u(\boldsymbol{M}(s), \boldsymbol{\Delta}(s))||_{2,\bar{\omega}}^2 > \int_{-\bar{\omega}}^{\bar{\omega}} \operatorname{tr}(\boldsymbol{Y}(\omega)) \frac{d\omega}{2\pi} \tag{17}$$

Eventually, recalling Eq. (10), Eq. (17) yields

$$||\boldsymbol{\mathcal{F}}_u(\boldsymbol{M}(s), \boldsymbol{\Delta}(s))||_{2,\bar{\omega}} > \gamma_l \quad \forall \boldsymbol{\Delta} \in \boldsymbol{B}_{\triangle} \tag{18}$$

■

Theorems 1 and 2 still apply if $\bar{\omega}$ is replaced with ∞, in which case upper and lower bounds on the classical H_2 norm of Eq. (2) are obtained. Note that in this case a weak inequality shall be imposed on the lower-right block of Eq. (6) and Eq. (9) to have $\operatorname{tr}(\boldsymbol{Y}(\omega)) \in \mathcal{L}_1(\mathbb{R})$, where $\mathcal{L}_1(\mathbb{R})$ is the space of real-valued functions whose absolute value is Lebesgue integrable [7].

IV. HAMILTONIAN-BASED METHOD

The LMIs defined in Theorems 1 and 2 are frequency-dependent, which requires solving an infinite-dimensional problem. To make it finite, Eq. (6) or (9) is first solved at a particular frequency ω_i, and a Hamiltonian-based technique is then used to determine the largest frequency interval $\bar{I}(\omega_i)$ on which the solution obtained at ω_i is valid. This process is finally repeated until the union of all intervals covers the frequency range of interest. The method was initially formulated in the context of μ-analysis [10] and it has been applied by Garulli et al. for the computation of an upper bound on the robust H_2 norm without G scalings [1]. It is generalized in Section IV-A to take into account the G scalings in the upper bound condition, and adapted in Section IV-B to the lower bound condition. This is the second contribution of this paper.

A. Upper Bound

The Hamiltonian-based approach adopted by [1] is now modified to include the G-scaling matrix.

Theorem 3: Let $\boldsymbol{M}(s) = \left[\begin{array}{c|c} \boldsymbol{A} & \boldsymbol{B} \\ \hline \boldsymbol{C} & \boldsymbol{D} \end{array}\right]$ and let $\tilde{\boldsymbol{D}}_i = \begin{bmatrix} \boldsymbol{X}_i^{1/2} & \boldsymbol{0} \\ \boldsymbol{0} & \boldsymbol{I} \end{bmatrix}$, $\tilde{\boldsymbol{G}}_i = \begin{bmatrix} \boldsymbol{G}_i & \boldsymbol{0} \\ \boldsymbol{0} & \boldsymbol{0} \end{bmatrix}$ and $\tilde{\boldsymbol{Y}}_i = \begin{bmatrix} \boldsymbol{I} & \boldsymbol{0} \\ \boldsymbol{0} & \boldsymbol{Y}_i \end{bmatrix}$, where $\boldsymbol{X}_i$, $\boldsymbol{G}_i$ and $\boldsymbol{Y}_i$ satisfy Eq. (6) for $\omega = \omega_i$. Define

$$\boldsymbol{\mathcal{H}} = \boldsymbol{A}_H - \boldsymbol{B}_H \boldsymbol{D}_H^{-1} \boldsymbol{C}_H \tag{19}$$

where

$$\boldsymbol{A}_H = \operatorname{diag}\left(\begin{bmatrix} \boldsymbol{A}_D & \boldsymbol{0} \\ \boldsymbol{C}_D^* \boldsymbol{C}_D & -\boldsymbol{A}_D^* \end{bmatrix}, \boldsymbol{A}_G, -\boldsymbol{A}_G^* \right) \tag{20}$$

$$\boldsymbol{B}_H = \begin{bmatrix} \boldsymbol{B}_D \\ \boldsymbol{C}_D^* \boldsymbol{D}_D \\ \boldsymbol{B}_G \\ j\boldsymbol{C}_G^* \end{bmatrix} \tag{21}$$

$$\boldsymbol{C}_H = \begin{bmatrix} \boldsymbol{D}_D^* \boldsymbol{C}_D & -\boldsymbol{B}_D^* & j\boldsymbol{C}_G & \boldsymbol{B}_G^* \end{bmatrix} \tag{22}$$

$$\boldsymbol{D}_H = \boldsymbol{D}_D^* \boldsymbol{D}_D + j\boldsymbol{D}_G - j\boldsymbol{D}_G^* - \tilde{\boldsymbol{Y}}_i \tag{23}$$

and

$$\begin{bmatrix} \boldsymbol{A}_D & \boldsymbol{B}_D \\ \boldsymbol{C}_D & \boldsymbol{D}_D \end{bmatrix} = \begin{bmatrix} \boldsymbol{A} - j\omega_i \boldsymbol{I} & \boldsymbol{B}\tilde{\boldsymbol{D}}_i^{-1} \\ \tilde{\boldsymbol{D}}_i \boldsymbol{C} & \tilde{\boldsymbol{D}}_i \boldsymbol{D} \tilde{\boldsymbol{D}}_i^{-1} \end{bmatrix} \tag{24}$$

$$\begin{bmatrix} \boldsymbol{A}_G & \boldsymbol{B}_G \\ \boldsymbol{C}_G & \boldsymbol{D}_G \end{bmatrix} = \begin{bmatrix} \boldsymbol{A} - j\omega_i \boldsymbol{I} & \boldsymbol{B}\tilde{\boldsymbol{D}}_i^{-1} \\ \tilde{\boldsymbol{D}}_i^{-1}\tilde{\boldsymbol{G}}_i\boldsymbol{C} & \tilde{\boldsymbol{D}}_i^{-1}\tilde{\boldsymbol{G}}_i\boldsymbol{D}\tilde{\boldsymbol{D}}_i^{-1} \end{bmatrix} \tag{25}$$

Define $\underline{\delta_\omega}$ and $\overline{\delta_\omega}$ as

$$\underline{\delta_\omega} = \begin{cases} -\omega_i \text{ if } j\boldsymbol{\mathcal{H}} \text{ has no positive real eigenvalues} \\ \max\left(\lambda \in \mathbb{R}_- : \det\left(\lambda \boldsymbol{I} + j\boldsymbol{\mathcal{H}}\right) = 0\right) \end{cases}$$

$$\overline{\delta_\omega} = \begin{cases} \infty \text{ if } j\boldsymbol{\mathcal{H}} \text{ has no negative real eigenvalues} \\ \min\left(\lambda \in \mathbb{R}_+ : \det\left(\lambda \boldsymbol{I} + j\boldsymbol{\mathcal{H}}\right) = 0\right) \end{cases}$$

Then $\boldsymbol{X}_i$, $\boldsymbol{G}_i$ and $\boldsymbol{Y}_i$ satisfy Eq. (6) $\forall \omega \in \bar{I}(\omega_i) = \left(\omega_i + \underline{\delta_\omega},\, \omega_i + \overline{\delta_\omega}\right)$.

Proof: The above result holds iff

$$\boldsymbol{\psi}(\omega_i + \delta_\omega) = \boldsymbol{\psi}(\omega) \prec \boldsymbol{0} \quad \forall \delta_\omega \in \left(\underline{\delta_\omega},\, \overline{\delta_\omega}\right) \tag{26}$$

with $\boldsymbol{\psi}(\omega) = \tilde{\boldsymbol{D}}_i^{-1}\boldsymbol{M}(j\omega)^* \tilde{\boldsymbol{D}}_i\tilde{\boldsymbol{D}}_i\boldsymbol{M}(j\omega)\tilde{\boldsymbol{D}}_i^{-1} + j\left(\tilde{\boldsymbol{D}}_i^{-1}\tilde{\boldsymbol{G}}_i\boldsymbol{M}(j\omega)\tilde{\boldsymbol{D}}_i^{-1} - \tilde{\boldsymbol{D}}_i^{-1}\boldsymbol{M}(j\omega)^*\tilde{\boldsymbol{G}}_i\tilde{\boldsymbol{D}}_i^{-1}\right) - \tilde{\boldsymbol{Y}}_i$. After standard matrix manipulations, one obtains (where, for better clarity, $\times$ denotes the standard matrix product)

$$\begin{aligned} \boldsymbol{\psi}(\omega) = \tilde{\boldsymbol{D}}_i^{-1}&\left(\boldsymbol{B}'\left(-j\omega\boldsymbol{I} - \boldsymbol{A}'\right)^{-1}\boldsymbol{C}' + \boldsymbol{D}'\right)\tilde{\boldsymbol{D}}_i \\ &\times\tilde{\boldsymbol{D}}_i\left(\boldsymbol{C}\left(j\omega\boldsymbol{I} - \boldsymbol{A}\right)^{-1}\boldsymbol{B} + \boldsymbol{D}\right)\tilde{\boldsymbol{D}}_i^{-1} \\ &+j\left(\tilde{\boldsymbol{D}}_i^{-1}\tilde{\boldsymbol{G}}_i\left(\boldsymbol{C}\left(j\omega\boldsymbol{I} - \boldsymbol{A}\right)^{-1}\boldsymbol{B} + \boldsymbol{D}\right)\tilde{\boldsymbol{D}}_i^{-1}\right) \\ &-j\left(\tilde{\boldsymbol{D}}_i^{-1}\left(\boldsymbol{B}'\left(-j\omega\boldsymbol{I} - \boldsymbol{A}'\right)^{-1}\boldsymbol{C}' + \boldsymbol{D}'\right)\tilde{\boldsymbol{G}}_i\tilde{\boldsymbol{D}}_i^{-1}\right) \\ &-\tilde{\boldsymbol{Y}}_i \\ = &\left(\boldsymbol{B}_D^*\left(-j\delta_\omega\boldsymbol{I} - \boldsymbol{A}_D^*\right)^{-1}\boldsymbol{C}_D^* + \boldsymbol{D}_D^*\right) \\ &\times\left(\boldsymbol{C}_D\left(j\delta_\omega\boldsymbol{I} - \boldsymbol{A}_D\right)^{-1}\boldsymbol{B}_D + \boldsymbol{D}_D\right) \\ &+j\left(\boldsymbol{C}_G\left(j\delta_\omega\boldsymbol{I} - \boldsymbol{A}_G\right)^{-1}\boldsymbol{B}_G + \boldsymbol{D}_G\right) \\ &-j\left(\boldsymbol{B}_G^*\left(-j\delta_\omega\boldsymbol{I} - \boldsymbol{A}_G^*\right)^{-1}\boldsymbol{C}_G^* + \boldsymbol{D}_G^*\right) \\ &-\tilde{\boldsymbol{Y}}_i \\ = &\boldsymbol{C}_H\left(j\delta_\omega\boldsymbol{I} - \boldsymbol{A}_H\right)^{-1}\boldsymbol{B}_H + \boldsymbol{D}_H \end{aligned}$$

Observing that $\forall\delta_\omega \in \left(\underline{\delta_\omega},\, \overline{\delta_\omega}\right)$, $\boldsymbol{\psi}(\omega_i + \delta_\omega) \prec \boldsymbol{0}$, the boundaries of the interval are obtained when $\det\left(\boldsymbol{\psi}(\omega_i + \delta_\omega)\right) = 0$, which holds iff

$$\det\left(\boldsymbol{C}_H\left(j\delta_\omega\boldsymbol{I} - \boldsymbol{A}_H\right)^{-1}\boldsymbol{B}_H + \boldsymbol{D}_H\right) = 0 \tag{27}$$

or, equivalently

$$\det\left(\boldsymbol{D}_H^{-1/2}\boldsymbol{C}_H\left(j\delta_\omega\boldsymbol{I} - \boldsymbol{A}_H\right)^{-1}\boldsymbol{B}_H\boldsymbol{D}_H^{-1/2} + \boldsymbol{I}\right) = 0 \tag{28}$$

and finally, from Sylvester's identity

$$\det\left(\left(j\delta_\omega\boldsymbol{I} - \boldsymbol{A}_H\right)^{-1}\boldsymbol{B}_H\boldsymbol{D}_H^{-1}\boldsymbol{C}_H + \boldsymbol{I}\right) = 0 \tag{29}$$

which also reads

$$\det\left(j\delta_\omega\boldsymbol{I} - \left(\boldsymbol{A}_H - \boldsymbol{B}_H\boldsymbol{D}_H^{-1}\boldsymbol{C}_H\right)\right) = 0 \tag{30}$$

Eventually, recalling the definition of $\boldsymbol{\mathcal{H}}$, Eq. (30) can be rearranged as

$$\det\left(\delta_\omega\boldsymbol{I} + j\boldsymbol{\mathcal{H}}\right) = 0 \tag{31}$$

■

B. Lower Bound

A similar procedure can be conducted for the lower-bound condition expressed in Theorem 2.

Theorem 4: Let $\boldsymbol{M}(s) = \left[\begin{array}{c|c} \boldsymbol{A} & \boldsymbol{B} \\ \hline \boldsymbol{C} & \boldsymbol{D} \end{array}\right]$ and let $\tilde{\boldsymbol{D}}_{i_+} = \begin{bmatrix} \boldsymbol{X}_i^{1/2} & \boldsymbol{0} \\ \boldsymbol{0} & \boldsymbol{I} \end{bmatrix}$, $\tilde{\boldsymbol{D}}_{i_-} = \begin{bmatrix} -\boldsymbol{X}_i^{1/2} & \boldsymbol{0} \\ \boldsymbol{0} & \boldsymbol{I} \end{bmatrix}$, $\tilde{\boldsymbol{G}}_i = \begin{bmatrix} \boldsymbol{G}_i & \boldsymbol{0} \\ \boldsymbol{0} & \boldsymbol{0} \end{bmatrix}$ and $\tilde{\boldsymbol{Y}}_i = \begin{bmatrix} -\boldsymbol{I} & \boldsymbol{0} \\ \boldsymbol{0} & \boldsymbol{Y}_i \end{bmatrix}$, where $\boldsymbol{X}_i$, $\boldsymbol{G}_i$ and $\boldsymbol{Y}_i$ satisfy Eq. (9) for $\omega = \omega_i$. Define

$$\boldsymbol{\mathcal{H}} = \boldsymbol{A}_H - \boldsymbol{B}_H\boldsymbol{D}_H^{-1}\boldsymbol{C}_H \tag{32}$$

where

$$\boldsymbol{A}_H = \operatorname{diag}\left(\begin{bmatrix} \boldsymbol{A}_{D_+} & \boldsymbol{0} \\ \boldsymbol{C}_{D_-}^*\boldsymbol{C}_{D_+} & -\boldsymbol{A}_{D_-}^* \end{bmatrix}, \boldsymbol{A}_G, -\boldsymbol{A}_G^*\right) \tag{33}$$

$$\boldsymbol{B}_H = \begin{bmatrix} \boldsymbol{B}_{D_+} \\ \boldsymbol{C}_{D_-}^*\boldsymbol{D}_{D_+} \\ \boldsymbol{B}_G \\ j\boldsymbol{C}_G^* \end{bmatrix} \tag{34}$$

$$\boldsymbol{C}_H = \begin{bmatrix} \boldsymbol{D}_{D_-}^*\boldsymbol{C}_{D_+} & -\boldsymbol{B}_{D_-}^* & j\boldsymbol{C}_G & \boldsymbol{B}_G^* \end{bmatrix} \tag{35}$$

$$\boldsymbol{D}_H = \boldsymbol{D}_{D_-}^*\boldsymbol{D}_{D_+} + j\boldsymbol{D}_G - j\boldsymbol{D}_G^* - \tilde{\boldsymbol{Y}}_i \tag{36}$$

and

$$\begin{bmatrix} \boldsymbol{A}_{D_+} & \boldsymbol{B}_{D_+} \\ \boldsymbol{C}_{D_+} & \boldsymbol{D}_{D_+} \end{bmatrix} = \begin{bmatrix} \boldsymbol{A} - j\omega_i\boldsymbol{I} & \boldsymbol{B}\tilde{\boldsymbol{D}}_{i_+}^{-1} \\ \tilde{\boldsymbol{D}}_{i_+}\boldsymbol{C} & \tilde{\boldsymbol{D}}_{i_+}\boldsymbol{D}\tilde{\boldsymbol{D}}_{i_+}^{-1} \end{bmatrix} \tag{37}$$

$$\begin{bmatrix} \boldsymbol{A}_{D_-} & \boldsymbol{B}_{D_-} \\ \boldsymbol{C}_{D_-} & \boldsymbol{D}_{D_-} \end{bmatrix} = \begin{bmatrix} \boldsymbol{A} - j\omega_i\boldsymbol{I} & \boldsymbol{B}\tilde{\boldsymbol{D}}_{i_+}^{-1} \\ \tilde{\boldsymbol{D}}_{i_-}\boldsymbol{C} & \tilde{\boldsymbol{D}}_{i_-}\boldsymbol{D}\tilde{\boldsymbol{D}}_{i_+}^{-1} \end{bmatrix} \tag{38}$$

$$\begin{bmatrix} \boldsymbol{A}_G & \boldsymbol{B}_G \\ \boldsymbol{C}_G & \boldsymbol{D}_G \end{bmatrix} = \begin{bmatrix} \boldsymbol{A} - j\omega_i\boldsymbol{I} & \boldsymbol{B}\tilde{\boldsymbol{D}}_{i_+}^{-1} \\ \tilde{\boldsymbol{D}}_{i_+}^{-1}\tilde{\boldsymbol{G}}_i\boldsymbol{C} & \tilde{\boldsymbol{D}}_{i_+}^{-1}\tilde{\boldsymbol{G}}_i\boldsymbol{D}\tilde{\boldsymbol{D}}_{i_+}^{-1} \end{bmatrix} \tag{39}$$

Define $\overline{\delta_\omega}$ and $\underline{\delta_\omega}$ as

$$\underline{\delta_\omega} = \begin{cases} -\omega_i \text{ if } j\boldsymbol{\mathcal{H}} \text{ has no positive real eigenvalues} \\ \max\left(\lambda \in \mathbb{R}_- : \det\left(\lambda \boldsymbol{I} + j\boldsymbol{\mathcal{H}}\right) = 0\right) \end{cases}$$

$$\overline{\delta_\omega} = \begin{cases} \infty \text{ if } j\boldsymbol{\mathcal{H}} \text{ has no negative real eigenvalues} \\ \min\left(\lambda \in \mathbb{R}_+ : \det\left(\lambda \boldsymbol{I} + j\boldsymbol{\mathcal{H}}\right) = 0\right) \end{cases}$$

Then $\boldsymbol{X}_i$, $\boldsymbol{G}_i$ and $\boldsymbol{Y}_i$ satisfy Eq. (9) $\forall \omega \in \bar{I}(\omega_i) = \left(\omega_i + \underline{\delta_\omega},\, \omega_i + \overline{\delta_\omega}\right)$.

Proof: The above solution holds iff

$$\boldsymbol{\psi}(\omega_i + \delta_\omega) = \boldsymbol{\psi}(\omega) \succ \boldsymbol{0} \quad \forall \delta_\omega \in \left(\underline{\delta_\omega},\, \overline{\delta_\omega}\right) \tag{40}$$

with $\boldsymbol{\psi}(\omega) = \tilde{\boldsymbol{D}}_{i_+}^{-1}\boldsymbol{M}(j\omega)^*\tilde{\boldsymbol{D}}_{i_-}\tilde{\boldsymbol{D}}_{i_+}\boldsymbol{M}(j\omega)\tilde{\boldsymbol{D}}_{i_+}^{-1} + j\left(\tilde{\boldsymbol{D}}_{i_+}^{-1}\tilde{\boldsymbol{G}}_i\boldsymbol{M}(j\omega)\tilde{\boldsymbol{D}}_{i_+}^{-1} - \tilde{\boldsymbol{D}}_{i_+}^{-1}\boldsymbol{M}(j\omega)^*\tilde{\boldsymbol{G}}_i\tilde{\boldsymbol{D}}_{i_+}^{-1}\right) - \tilde{\boldsymbol{Y}}_i$. After a few matrix manipulations, one obtains

$$\begin{aligned}\boldsymbol{\psi}(\omega) &= \tilde{\boldsymbol{D}}_{i_+}^{-1}\left(\boldsymbol{B}'\left(-j\omega\boldsymbol{I}-\boldsymbol{A}'\right)^{-1}\boldsymbol{C}'+\boldsymbol{D}'\right)\tilde{\boldsymbol{D}}_{i_-}\\ &\quad\times\tilde{\boldsymbol{D}}_{i_+}\left(\boldsymbol{C}\left(j\omega\boldsymbol{I}-\boldsymbol{A}\right)^{-1}\boldsymbol{B}+\boldsymbol{D}\right)\tilde{\boldsymbol{D}}_{i_+}^{-1}\\ &\quad+j\left(\tilde{\boldsymbol{D}}_{i_+}^{-1}\tilde{\boldsymbol{G}}_i\left(\boldsymbol{C}\left(j\omega\boldsymbol{I}-\boldsymbol{A}\right)^{-1}\boldsymbol{B}+\boldsymbol{D}\right)\tilde{\boldsymbol{D}}_{i_+}^{-1}\right)\\ &\quad-j\left(\tilde{\boldsymbol{D}}_{i_+}^{-1}\left(\boldsymbol{B}'\left(-j\omega\boldsymbol{I}-\boldsymbol{A}'\right)^{-1}\boldsymbol{C}'+\boldsymbol{D}'\right)\tilde{\boldsymbol{G}}_i\tilde{\boldsymbol{D}}_{i_+}^{-1}\right)\\ &\quad-\tilde{\boldsymbol{Y}}_i\\ &= \left(\boldsymbol{B}_{D_-}^*\left(-j\delta_\omega\boldsymbol{I}-\boldsymbol{A}_{D_-}^*\right)^{-1}\boldsymbol{C}_{D_-}^*+\boldsymbol{D}_{D_-}^*\right)\\ &\quad\times\left(\boldsymbol{C}_{D_+}\left(j\delta_\omega\boldsymbol{I}-\boldsymbol{A}_{D_+}\right)^{-1}\boldsymbol{B}_{D_+}+\boldsymbol{D}_{D_+}\right)\\ &\quad+j\left(\boldsymbol{C}_G\left(j\delta_\omega\boldsymbol{I}-\boldsymbol{A}_G\right)^{-1}\boldsymbol{B}_G+\boldsymbol{D}_G\right)\\ &\quad-j\left(\boldsymbol{B}_G^*\left(-j\delta_\omega\boldsymbol{I}-\boldsymbol{A}_G^*\right)^{-1}\boldsymbol{C}_G^*+\boldsymbol{D}_G^*\right)\\ &\quad-\tilde{\boldsymbol{Y}}_i\\ &= \boldsymbol{C}_H\left(j\delta_\omega\boldsymbol{I}-\boldsymbol{A}_H\right)^{-1}\boldsymbol{B}_H+\boldsymbol{D}_H\end{aligned}$$

from which the result follows in the same way as for Theorem 3. ■

V. PRACTICAL ALGORITHM

This section formalizes the proposed algorithm to compute guaranteed lower and upper bounds on the finite-frequency H_2 norm of the uncertain MIMO linear system of Fig. 1. The frequency range of interest $I_d = [-\bar{\omega}, \bar{\omega}]$ is divided into n disjoint intervals $I(\omega_i)$ centered around the frequencies ω_i, and $2n$ SDP optimization problems are solved. Let $\boldsymbol{M}_i = \boldsymbol{M}(\omega_i)$. The computation of γ_u is performed by minimizing the trace of $\boldsymbol{Y}(\omega)$ at each frequency ω_i:

$$\min_{\boldsymbol{X}_i,\boldsymbol{G}_i,\boldsymbol{Y}_i} \operatorname{tr}(\boldsymbol{Y}_i) \tag{41}$$

subject to

$$\begin{aligned}&\boldsymbol{M}_i^*\begin{bmatrix}\boldsymbol{X}_i & \boldsymbol{0}\\ \boldsymbol{0} & \boldsymbol{I}\end{bmatrix}\boldsymbol{M}_i - \begin{bmatrix}\boldsymbol{X}_i & \boldsymbol{0}\\ \boldsymbol{0} & \boldsymbol{Y}_i\end{bmatrix}\\ &+j\left(\begin{bmatrix}\boldsymbol{G}_i & \boldsymbol{0}\\ \boldsymbol{0} & \boldsymbol{0}\end{bmatrix}\boldsymbol{M}_i - \boldsymbol{M}_i^*\begin{bmatrix}\boldsymbol{G}_i & \boldsymbol{0}\\ \boldsymbol{0} & \boldsymbol{0}\end{bmatrix}\right) \prec \boldsymbol{0}\end{aligned} \tag{42}$$

Similarly, γ_l is computed by maximizing the trace of $\boldsymbol{Y}(\omega)$ at each frequency ω_i:

$$\max_{\boldsymbol{X}_i,\boldsymbol{G}_i,\boldsymbol{Y}_i} \operatorname{tr}(\boldsymbol{Y}_i) \tag{43}$$

subject to

$$\begin{aligned}&\boldsymbol{M}_i^*\begin{bmatrix}-\boldsymbol{X}_i & \boldsymbol{0}\\ \boldsymbol{0} & \boldsymbol{I}\end{bmatrix}\boldsymbol{M}_i - \begin{bmatrix}-\boldsymbol{X}_i & \boldsymbol{0}\\ \boldsymbol{0} & \boldsymbol{Y}_i\end{bmatrix}\\ &+j\left(\begin{bmatrix}\boldsymbol{G}_i & \boldsymbol{0}\\ \boldsymbol{0} & \boldsymbol{0}\end{bmatrix}\boldsymbol{M}_i - \boldsymbol{M}_i^*\begin{bmatrix}\boldsymbol{G}_i & \boldsymbol{0}\\ \boldsymbol{0} & \boldsymbol{0}\end{bmatrix}\right) \succ \boldsymbol{0}\end{aligned} \tag{44}$$

Frequency intervals $\bar{I}(\omega_i)$ on which the solutions obtained at ω_i remain valid are then computed through the Hamiltonian-based technique of Section IV. If $I(\omega_i) \subset \bar{I}(\omega_i)$ for all i, two step-wise functions are obtained, which delimit from above and below all possible values of $\operatorname{tr}\left(\boldsymbol{\mathcal{F}}_u(j\omega)\boldsymbol{\mathcal{F}}_u(j\omega)^*\right)$. Otherwise, the intervals such that $I(\omega_i) \not\subseteq \bar{I}(\omega_i)$ are divided into smaller ones as explained in Algorithm 1 and the whole process is repeated. γ_u and γ_l are finally determined by integrating the step-wise functions over I_d:

$$\sum_{i=1}^{n}\int_{\omega\in I(\omega_i)} \operatorname{tr}(\boldsymbol{Y}_i(\omega))\,\frac{d\omega}{2\pi} \tag{45}$$

The number n of intervals $I(\omega_i)$ allows handling the trade off between accuracy and computational time. A larger n means a longer computational time, but also a larger number of steps for the bounding functions, i.e. a better accuracy.

Algorithm 1 Finite-frequency H_2-norm analysis of uncertain MIMO linear systems.

1: Divide I_d into disjoint intervals $I(\omega_i)$ with centre in ω_i
2: **for** all $I(\omega_i)$ **do**
3: Solve the SDP optimization problem (41)-(42) or (43)-(44) at frequency ω_i
4: Compute the largest frequency range $\bar{I}(\omega_i)$ for which the LMIs are valid with the Hamiltonian-based technique
5: **if** $I(\omega_i) \not\subseteq \bar{I}(\omega_i)$ **then**
6: **while** $\exists\, I(\omega_{ik}) \not\subseteq \bar{I}(\omega_{ik})$ and the number of frequency intervals $I(\omega_{ik})$ is lower than a threshold **do**
7: Divide $I(\omega_i)$ into a finer partition $\bigcup_k I(\omega_{ik})$ and repeat Steps 3 and 4
8: **end while**
9: **if** still $\exists\, I(\omega_{ik}) \not\subseteq \bar{I}(\omega_{ik})$ **then**
10: **while** $I(\omega_{ik}) \not\subseteq \bar{I}(\omega_{ik})$ **do**
11: Solve the SDP optimization problem imposing the LMIs on an increasing number of frequency points in $I(\omega_{ik})$
12: Repeat Step 4
13: **end while**
14: **end if**
15: **end if**
16: **end for**
17: Compute an upper or a lower bound on the finite-frequency H_2 norm with Eq. (45)

VI. APPLICATIONS

All results have been obtained using LMILAB on a Windows 10 laptop with a 13th Gen Intel(R) Core(TM) i5-1345U as CPU and 16 GB of RAM.

A. Validation Example

Algorithm 1 is first validated against the Single-Input Single-Output (SISO) system taken from [1]. The LFT has a single real parametric uncertainty repeated twice and state-space matrices as follows:

$$\boldsymbol{A} = \begin{bmatrix}-2.5 & 0.5 & 0 & -50 & 0\\ 0 & -1 & 0.5 & 0 & 0\\ 0 & -0.5 & 0 & 0 & 0\\ 0 & 0 & 0 & -5 & 100\\ 0 & 0 & 0 & -100 & 0\end{bmatrix}$$

$$\boldsymbol{B} = \begin{bmatrix} 0.25 & -0.5 & 0 \\ 0 & 0 & 5 \\ 0 & 0 & 0 \\ 0 & 0 & 0 \\ 0 & 0 & 5 \end{bmatrix}$$

$$\boldsymbol{C} = \begin{bmatrix} 1 & 0 & 0 & 0 & 0 \\ 0 & 0 & 0 & 0 & 0 \\ 1 & 0 & 0 & 0 & 0 \end{bmatrix}, \quad \boldsymbol{D} = \begin{bmatrix} 0 & 0 \\ 1 & 0 \\ 0 & 0 \end{bmatrix}$$

The upper bound on the considered frequency range is set to $\bar{\omega} = 50$ rad/s. As in [1], the frequency range of interest is initially divided into 200 equispaced intervals $I(\omega_i)$, whereas the uncertainty domain is not partitioned. The results produced by Algorithm 1 are presented in Table I, where they are compared with the outcome of [1].

TABLE I

RESULTS COMPARISON FOR THE VALIDATION EXAMPLE.

	New results	Results from [1]
Upper bound	0.950	1.186
Lower bound	0.844	-
Time [s]	16.1	144

The implemented algorithm is much faster with respect to the one proposed in [1]. The accuracy of the upper bound, furthermore, is increased thanks to the introduction of the G scalings. It is normal for the gap between the bounds to be large. A strong dispersion of the frequency response is indeed observed in Fig. 2 when the uncertainty varies between its min and max values. On the other hand, it can be seen that the proposed algorithm is not very conservative, since the gap between the calculated step-wise bounds on $|\mathcal{F}_u(j\omega)|^2$ and the samples is very small. The smallest (resp. largest) frequency-limited H_2 norm calculated on all samples is 0.848 (resp. 0.892). It is very close to the lower (resp. upper) bound shown in Table I.

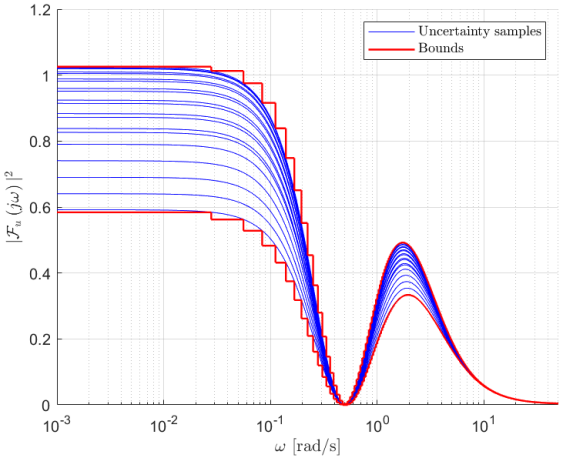

Fig. 2. Bounds on $|\mathcal{F}_u(j\omega)|^2$: validation example.

B. Satellite Benchmark

The effectiveness of the proposed implementation is then tested on a more demanding satellite benchmark taken from [18]. Since coupling effects are often negligible, the satellite is represented as a single-axis model. Let θ be the attitude angle of the satellite and $J = 1000$ kg m^2 its nominal moment of inertia [18]. The SISO dynamics of the model can be expressed as

$$J\ddot{\theta} = T_W + T_S + T_F + T_D \tag{46}$$

where T_W is the control input torque, T_S is induced by the propellant slosh effects, T_F is produced by the flexible modes of the solar arrays and T_D includes all remaining disturbance torques. As it is common in the literature, T_S and T_F are represented as poorly damped second-order linear models:

$$T_S + T_F = \sum_i \frac{L_i s^2}{s^2 + 2\xi_i\omega_i s + \omega_i^2}\ddot{\theta} \tag{47}$$

where L_i, ω_i and ξ_i indicate respectively the magnitude, the frequency and the damping of the i-th mode. Their nominal values are reported in Table II [18].

TABLE II

SLOSH AND FLEXIBLE MODES PARAMETERS (NOMINAL VALUES) [18].

Mode	L_i [kg m^2]	ω_i [rad/s]	ξ_i
1	30	0.1	5×10^{-3}
2	40	0.2	4×10^{-3}
3	50	0.3	3×10^{-3}
4	300	0.6	1×10^{-3}
5	100	1	1×10^{-3}

The control input torque T_W, furthermore, is generated from the commanded torque T_C by a reaction wheel, which can be approximated as a first-order linear model with a time constant $\tau = 0.5$ s:

$$T_W = \frac{1}{1+\tau s} T_C \tag{48}$$

A 5-th order controller is designed to ensure closed-loop stability and reject as much as possible the disturbance torques T_D. The transfer between T_D and θ is considered for H_2 performance analysis.

Algorithm 1 is first tested on the rigid satellite model, which includes only uncertainties on the inertia and the time constant. Then, more complex systems are obtained by adding one by one the slosh and flexible modes reported in Table II. Each mode is supposed to carry three uncertainties: one on the magnitude, another on the damping and a last one on the frequency, the latter being repeated twice. In this way it is possible to implement 6 models of the spacecraft which have an increasing number of uncertainties. Each uncertain parameter is allowed to vary independently from the others by $\pm 11\%$ around its nominal value. Note that Model 6 is no longer stable on the entire uncertainty domain if the uncertainties vary by $\pm 12\%$ around the nominal condition [18]. Setting $\bar{\omega} = 3$ rad/s, the frequency range of interest I_d

is initially partitioned into 100 equispaced intervals $I(\omega_i)$. The results of the H_2 performance analysis obtained with Algorithm 1 are reported in Table III, where n_u, d and n respectively indicate the number of uncertainties, the dimension of $\boldsymbol{\Delta}$ and the number of states of $\boldsymbol{M}(s) = \left[\begin{array}{c|c} \boldsymbol{A} & \boldsymbol{B} \\ \hline \boldsymbol{C} & \boldsymbol{D} \end{array}\right]$.

TABLE III

RESULTS COMPARISON FOR THE SATELLITE BENCHMARK.

Model	n_u	d	n	γ_l	γ_u	Time [s]
1	2	2	9	3.0×10^{-3}	4.0×10^{-3}	3.6
2	5	6	11	3.0×10^{-3}	4.0×10^{-3}	11.6
3	8	10	13	2.8×10^{-3}	4.2×10^{-3}	32.0
4	11	14	15	2.6×10^{-3}	4.5×10^{-3}	80.2
5	14	18	17	2.0×10^{-3}	5.1×10^{-3}	184.7
6	17	22	19	1.9×10^{-3}	8.0×10^{-3}	311.1

The increase in the dimension of $\boldsymbol{\Delta}$ makes the algorithm slower as the number of decision variables increases. Table III, furthermore, shows that the gap between γ_l and γ_u increases with d. This result does not imply that the implemented algorithm is conservative, but it is due to the fact that the LFT frequency response $\mathcal{F}_u(j\omega)$ varies more on the global uncertainty domain.

Emblematic is the case of Model 6, where all modes reported in Table II are included. The μ-based H_∞-norm analysis of such a system has identified a peak at a frequency of 2.346 $\mathrm{rad/s}$ which was not present in the models with less uncertain parameters [18]. The peak was not identified by Monte Carlo simulations despite the fact that 10^5 samples were considered. Probabilistic μ-analysis, in fact, revealed that its probability of occurrence is extremely low (less than $10^{-4}\%$). It is interesting to note that Algorithm 1 is capable of identifying the peak as an increase in the step-wise upper bound on $|\mathcal{F}_u(j\omega)|^2$. Fig. 3 represents different samples of the LFT transfer function together with the upper and lower bounds computed by Algorithm 1. The green line corresponds to the worst H_∞-norm system identified with μ-analysis [18]. The computation of the upper bound is accurate as the step-wise function follows precisely the trend of the worst-case H_∞-norm system for the main peak. The gap between γ_l and γ_u, therefore, is mostly due to the scattering of $\mathcal{F}_u(j\omega)$ around its nominal value.

C. Probabilistic H_2-Norm Analysis

Consider now the following academic benchmark taken from [19]:

$$\begin{cases} \dot{\boldsymbol{x}} = \begin{bmatrix} 0 & 1 \\ -a_1(\delta_1) & -a_2(\delta_2) \end{bmatrix} \boldsymbol{x} + \begin{bmatrix} 0 \\ 1 \end{bmatrix} u \\ y = \begin{bmatrix} 1 & 0 \end{bmatrix} \boldsymbol{x} \end{cases} \tag{49}$$

with

$$\begin{cases} a_1(\delta_1) = 1 + 2\delta_1 \\ a_2(\delta_2) = 0.8 + \delta_2 \end{cases} \tag{50}$$

where δ_1 and δ_2 are normalized parametric uncertainties with truncated normal distribution on $[-1, 1]$, null mean and variance equal to 0.1. The objective is to analyze the H_2 performance of the system when $\bar{\omega} = 4$ $\mathrm{rad/s}$, and beyond that to compute the probability that a performance requirement is either matched or violated.

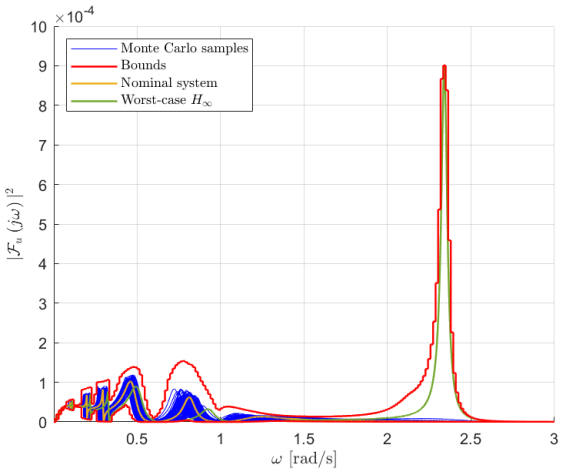

Fig. 3. Bounds on $|\mathcal{F}_u(j\omega)|^2$: satellite with 17 uncertainties.

As Algorithm 1 can compute both an upper and a lower bound on the H_2 norm of an uncertain system, it can be integrated into the Branch and Bound (B&B) scheme of Roos et al. [18]. The latter is implemented in the *mupb* function of the STOchastic Worst-case Analysis Toolbox (STOWAT) developed by ONERA with the support of ESA and CNES [18]. *mupb* divides the entire uncertainty domain into smaller and smaller boxes, and computes hard bounds on the probability that system performance is either satisfied or violated. The function performs first a stability analysis, which partitions the uncertainty domain D into the subsets of guaranteed stability D_s, guaranteed instability $D_{\bar{s}}$ and undetermined stability D_{s_u}: $D = D_s \cup D_{\bar{s}} \cup D_{s_u}$. Then, given a certain H_2 performance level, the B&B algorithm of *mupb* combined with Algorithm 1 partitions the stability domain D_s into the subsets of guaranteed performance D_γ, guaranteed non-performance $D_{\bar{\gamma}}$ and undetermined performance D_{γ_u}: $D = D_\gamma \cup D_{\gamma_u} \cup D_{\bar{\gamma}} \cup D_{\bar{s}} \cup D_{s_u}$. If the probability of each region of D is also computed, one obtains

$$p(D) = p(D_\gamma) + p(D_{\gamma_u}) + p(D_{\bar{\gamma}}) + p(D_{\bar{s}}) + p(D_{s_u}) \tag{51}$$

The probability that the considered performance level is satisfied is finally guaranteed to lie between $p(D_\gamma)$ and $p(D_\gamma) + p(D_{\gamma_u}) + p(D_{s_u})$.

Coming back to system (49)-(50), the H_2 performance threshold is first set to 0.8 and the frequency range of interest is initially partitioned into 500 equispaced intervals. The algorithm stops when the probability of each undetermined box is below $10^{-3}\%$. *mupb* takes ~ 5.4 hr to assess that the probability of $||\boldsymbol{\mathcal{F}}_u(\boldsymbol{M}(s), \boldsymbol{\Delta}(s))||_{2,\bar{\omega}} \leq 0.8$ is comprised between 45.0% and 46.5%. The probability of performance violation (namely $||\boldsymbol{\mathcal{F}}_u(\boldsymbol{M}(s), \boldsymbol{\Delta}(s))||_{2,\bar{\omega}} > 0.8$), instead, is guaranteed between 47.4% and 48.9%. Fig. 4 graphically

represents the partition of the uncertainty domain identified by *mupb*.

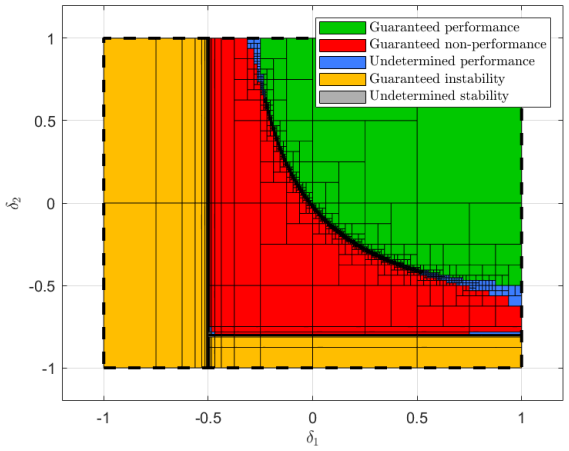

Fig. 4. Partitions of the uncertainty domain.

Note that the mentioned computational time should not be compared with the CPU times reported in Tables I and III, as in this example upper and lower bounds on $||\boldsymbol{\mathcal{F}}_u(\boldsymbol{M}(s), \boldsymbol{\Delta}(s))||_{2,\bar{\omega}}$ are computed on each partition of the uncertainty domain, i.e. thousands of times. The total computational time of *mupb*, furthermore, is greatly reduced when there is low probability that a given H_2 performance is violated, which is often the case for practical applications. To highlight this consideration, the H_2 performance threshold is now increased up to 6 and the frequency range of interest is initially partitioned into only 50 equispaced intervals. The algorithm is requested to stop when the probability of violation is guaranteed to be lower than 1%. *mupb* takes approximately 2.5 $\min$ to ensure that the probability of performance violation is comprised between $p(D_{\bar{\gamma}}) = 0.0\%$ and $p(D_{\bar{\gamma}}) + p(D_{\gamma_u}) + p(D_{s_u}) = 1.0\%$. The probability of performance satisfaction is instead comprised between 92.9% and 93.9%.

VII. CONCLUSIONS

A method is proposed in this paper to compute guaranteed lower and upper bounds on the H_2 norm of an uncertain linear system. Two main improvements have been gained with respect to existing literature. Firstly, a sufficient condition to compute a guaranteed lower bound has been demonstrated. Secondly, the accuracy of the existing upper bound has been significantly increased by the introduction of G scalings.

The proposed method is particularly interesting for different reasons. Primarily, its numerical implementation can be integrated in the B&B algorithm of the STOWAT to compute the probability that an H_2 performance requirement of an uncertain system is either satisfied or violated. Furthermore, the theoretical results presented in the paper can be extended to discrete-time systems. A sufficient condition to compute a lower bound on the robust H_∞ norm of an uncertain system can also be found by following the same approach. Such a condition would be valid for both SISO and MIMO systems, whereas current techniques concern SISO systems only [20]. Eventually, Theorem 1 and Theorem 2 can be straightforwardly generalized to include time-varying and non-linear uncertainties.

REFERENCES

[1] A. Garulli, A. Hansson, S. K. Pakazad, A. Masi, and R. Wallin, "Robust finite-frequency H_2 analysis of uncertain systems with application to flight comfort analysis," *Control Engineering Practice*, vol. 21, no. 5, pp. 887–897, 2013.

[2] D. Alazard, "Robust H_2 design for lateral flight control of highly flexible aircraft," *Journal of Guidance, Control, and Dynamics*, vol. 25, no. 3, pp. 502–510, 2002.

[3] R. Crarcciolo, D. Richiedei, and A. Trevisani, "Robust mixed-norm position and vibration control of flexible link mechanisms," *Mechatronics*, vol. 15, no. 7, pp. 767–791, 2005.

[4] E. Zattoni, "Detection of incipient failures by using an H_2-norm criterion: Application to railway switching points," *Control Engineering Practice*, vol. 14, no. 8, pp. 885–895, 2006.

[5] M. Martin, F. Belien, A. Falke, and R. Förstner, "Robust performance analysis using H_2-norm for quadcopter-based mobility on small bodies," in *Proceedings of the IEEE Aerospace Conference*, Big Sky, MT, USA, March 2021.

[6] D. Navarro-Tapia, A. Marcos, and J. Veenman, "Enhanced AOCS verification techniques for Euclid's high-pointing performance," *IFAC PapersOnLine*, vol. 55, no. 25, pp. 91–96, 2022.

[7] F. Paganini, "Convex methods for robust H_2 analysis of continuous-time systems," *IEEE Transactions on Automatic Control*, vol. 44, no. 2, pp. 239–252, 1999.

[8] F. Paganini, "Frequency domain conditions for robust H_2 performance," *IEEE Transactions on Automatic Control*, vol. 44, no. 1, pp. 38–49, 1999.

[9] C. Roos and J.-M. Biannic, "Efficient computation of a guaranteed stability domain for a high-order parameter dependent plant," in *Proceedings of the American Control Conference*, Baltimore, MD, USA, June 2010.

[10] G. Ferreres, "A μ analysis technique without frequency gridding," in *Proceedings of the American Control Conference*, Philadelphia, PA, USA, June 1998.

[11] C. W. Scherer and I. E. Köse, "Robustness with dynamic IQCs: An exact state space characterization of nominal stability with applications to robust estimation," *Automatica*, vol. 44, pp. 1666–1675, 2008.

[12] W. C. Scherer and I. E. Köse, "Robust H_2 estimation with dynamic IQCs: A convex solution," in *Proceedings of the 45th IEEE Conference on Decision & Control*, San Diego, CA, USA, December 2006.

[13] J. Veenman, C. W. Scherer, C. Ardura, S. Bennani, V. Preda, and B. Girouart, "IQClab: A new IQC based toolbox for robustness analysis and control design," *IFAC PapersOnLine*, vol. 54, no. 8, pp. 69–74, 2021.

[14] V. Preda, "Robust microvibration control and worst-case analysis for high pointing stability space missions," Ph.D. dissertation, Université de Bordeaux, December 2017.

[15] M. K. H. Fan, A. L. Tits, and J. C. Doyle, "Robustness in the presence of mixed parametric uncertainty and unmodelled dynamics," *IEEE Transactions on Automatic Control*, vol. 36, no. 1, pp. 25–38, 1991.

[16] C. Roos, "Advanced control laws design and validation - A set of methods and tools to bridge the gap between theory and practice," Habilitation à diriger des recherches, Université de Toulouse, April 2018.

[17] S. Boyd and C. Barratt, *Linear Controller Design: Limits of Performance*. Prentice-Hall, 1991.

[18] C. Roos, J.-M. Biannic, and H. Evain, "A new step towards the integration of probabilistic μ in the aerospace V&V process," *CEAS Space Journal*, vol. 16, pp. 59–71, 2023.

[19] A. Falcoz, D. Alazard, and C. Pittet, "Probabilistic μ-analysis for system performances assessment," *IFAC-PapersOnLine*, vol. 50, no. 1, pp. 399–404, July 2017.

[20] S. Thai, C. Roos, and J.-M. Biannic, "Probabilistic μ-analysis for stability and H_∞ performance verification," in *Proceedings of the American Control Conference*, Philadelphia, PA, USA, July 2019.